DALTON
FULL PAPER

Synthesis, crystal structures and dynamic behaviour of the pentanuclear mixed-metal cluster compounds [$Au_2Ru_3(\mu$-H)(μ_3-COMe){μ-$Ph_2P(CH_2)_nPPh_2$}$(CO)_9$] (n =1 or 5)‡

Catriona A. Collins,[a] **Ian D. Salter,***[†,a] **Vladimir Šik,**[a] **Steven A. Williams**[a] **and Trushar Adatia**[b]

[a] *Department of Chemistry, University of Exeter, Stocker Road, Exeter, UK EX4 4QD*
[b] *School of Biological and Applied Sciences, University of North London, Holloway Road, London, UK N7 8DB*

The cluster compound [$Ru_3(\mu$-H$)_3(\mu_3$-COMe)$(CO)_9$] reacted with the complex [Au_2{μ-$Ph_2P(CH_2)_nPPh_2$}Me_2] (n = 1 or 5) in diethyl ether solution to afford the new mixed-metal cluster compounds [$Au_2Ru_3(\mu$-H)(μ_3-COMe)-{μ-$Ph_2P(CH_2)_nPPh_2$}$(CO)_9$] (n = 1 **1** or 5 **2**) in *ca.* 30–40% yield. Compounds **1** and **2** have been characterized by IR and NMR spectroscopy and by single-crystal X-ray diffraction. The X-ray diffraction studies show that the Au_2Ru_3 metal cores of **1** and **2** both adopt similar distorted square-based pyramidal structures, with the basal plane defined by the two Au atoms and two of the Ru atoms and the third Ru atom forming the apex of the pyramid [Au–Au 2.878(1), Au–Ru 2.688(1)–2.863(1), Ru–Ru 2.887(1)–2.891(1) Å for **1** and Au–Au 3.109(1), Au–Ru 2.716(3)–2.787(3), Ru–Ru 2.859(2)–2.895(3) Å for **2**]. The $Ph_2P(CH)_nPPh_2$ (n = 1 or 5) ligand bridges the two Au atoms, the methoxycarbyne caps the Ru_3 face and the hydride bridges the basal Ru–Ru edge of the metal framework. Each ruthenium atom is bonded to three terminal carbonyl groups. Variable-temperature NMR spectroscopic studies suggested that the metal skeletons of **1** and **2** are stereochemically non-rigid at high temperature in solution. The novel fluxional process is thought to involve a migration of the diphosphinedigold group around the three possible edge-bridging sites on the trigonal-planar triruthenium unit, together with a concomitant movement of the edge-bridging hydride ligand. Band-shape analysis of variable-temperature ^1H and ^{13}C-{^1H} NMR spectra afforded values of $\Delta G^‡$ for these proposed metal-core rearrangements of 67.1 ± 0.2 (^1H) and 67.0 ± 0.2 kJ mol^{-1} (^{13}C-{^1H}) for **1** and 58.9 ± 0.1 kJ mol^{-1} (^{13}C-{^1H}) for **2**. These free energies of activation are surprisingly high compared with those previously reported for skeletal rearrangements in gold–ruthenium heteronuclear cluster compounds.

Heteronuclear cluster compounds containing $Au(ER_3)$ (E = As or P, R = alkyl or aryl) units have attracted considerable interest over the last fifteen years. A large number of examples of these species have now been synthesized and studied and, in the vast majority of cases, the gold atom(s) are ligated by organophosphine(s).[2–4] The $Au(ER_3)$ fragments in this class of cluster compound can adopt either edge-bridging or face-capping bonding modes on subunits of transition metals (M) other than Group IB metals. These subunits normally either consist of a discrete trigonal-planar M_3 unit or an M_3 face of a larger polyhedron of M atoms.[2–5] When two $Au(ER_3)$ groups are present in a cluster the situation is complicated by a tendency of the gold atoms to occupy adjacent sites in the metal framework, which has been attributed to bonding interactions between the gold atoms.[2,3,6,7] The energy differences between metal core structures with and without the gold atoms in close contact often seem to be small, so clusters containing two $Au(ER_3)$ units exhibit a wide range of skeletal geometries.[2,3] These can be classified into four main structural types, depending on whether the two $Au(ER_3)$ groups are edge-bridging or face-capping and whether or not there is a close contact between the gold atoms.[2,3] The most common metal core structure has two face-capping $Au(ER_3)$ units in close contact (gold arrangement A in Fig. 1).[2,3] Digold heteronuclear clusters containing two $Au(ER_3)$ fragments bridging different metal–metal edges with the gold atoms in close contact (gold arrangement B in Fig. 1) are very much rarer and most known examples have the Au atoms linked together by the bidentate ligands $Ph_2E(CH_2)_n$-$E'Ph_2$ (E = E′ = As or P; E = As, E′ = P; n = 1 or 2),[8–11] *cis*-$Ph_2PCH{=}CHPPh_2$[12,13] or Fe(η-$C_5H_4PPh_2)_2$.[1] Indeed, it has been proposed that it is actually the stereochemical demands of $Ph_2E(CH_2)_nE'Ph_2$, *cis*-$Ph_2PCH{=}CHPPh_2$ and Fe(η-$C_5H_4PPh_2)_2$ that cause heteronuclear clusters in which two gold atoms are bonded to these bidentate ligands to adopt skeletal geometries with gold arrangement B (Fig. 1).[1,8–13] This hypothesis is supported by the fact that the analogous clusters in which the bidentate ligand bonded to the gold atoms is formally replaced by two monodentate organophosphines are observed to adopt a different metal core structure, normally with gold arrangement A (Fig. 1).[14,15]

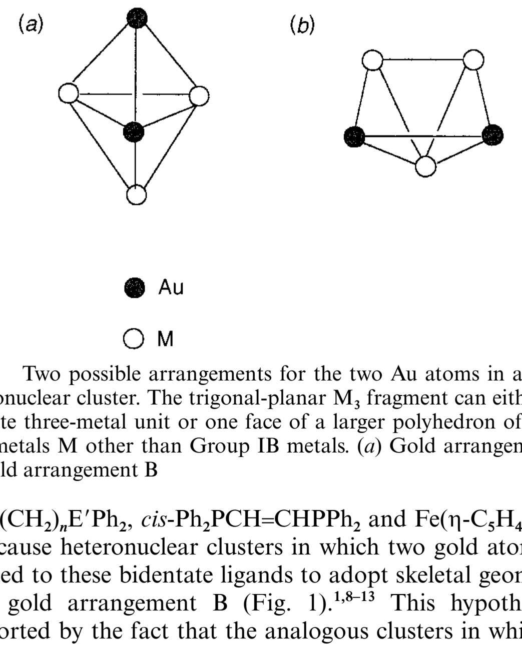

Fig. 1 Two possible arrangements for the two Au atoms in a digold heteronuclear cluster. The trigonal-planar M_3 fragment can either be a discrete three-metal unit or one face of a larger polyhedron of transition metals M other than Group IB metals. (*a*) Gold arrangement A, (*b*) gold arrangement B

In view of the results described above, the clusters [Au_2Ru_3-(μ-H)(μ_3-COMe)$(CO)_9(PPh_3)_2$],[16,17] [$Au_2Os_4(CO)_{12}L(PRR'_2)_2$][18] [L = CO, R = R′ = Ph or Et; L = CO, R = Me, R′ = Ph; L = P(OMe)$_3$, R = R′ = Et] and [$Au_2Os_4(CO)_{11}L_2(PEt_3)_2$][18] [L = P(OMe)$_3$ or CNBu^t] are very unusual, since they all adopt metal core structures with gold arrangement B, even though the gold atoms are ligated by monodentate phosphines rather than

---

[†] E-Mail: I.D.Salter@exeter.ac.uk

[‡] The heteronuclear cluster chemistry of the Group IB metals. Part 21.[1]

Table 1 Characterization of the new Group IB heteronuclear cluster compounds

(*a*) Analytical and physical data

Cluster compound	$\tilde{\nu}_{max}$(CO)[a]/cm^{-1}	Yield (%)[b]	M.p. (θ/°C) (decomp.)	Analysis (%)[c] C	H
1 $[Au_2Ru_3(\mu\text{-}H)(\mu_3\text{-}COMe)(\mu\text{-}Ph_2PCH_2PPh_2)(CO)_9]$	2064vs, 2036vs, 2022vs, 1984m, 1936m, 1920w(br)	31	147–149	31.8 (31.4)	1.8 (1.9)
2 $[Au_2Ru_3(\mu\text{-}H)(\mu_3\text{-}COMe)\{\mu\text{-}Ph_2P(CH_2)_5PPh_2\}(CO)_9]$	2062s, 2036vs, 2017vs, 1979m (br), 1915w (br)	38	156–159	33.2 (33.5)	2.4 (2.4)

(*b*) Hydrogen-1 and ^{31}P NMR data,[d] at +30 °C

Cluster	^{1}H NMR[e]	^{31}P-{^{1}H} NMR[e,f]
1	−18.89 [t, 1 H, μ-H, *J*(PH) 1], 3.47 [overlapping d of t, br, 1 H, PCH_2P, *J*(PH) 11, *J*(HH) 12], 3.81 [overlapping d of t, br, 1 H, PCH_2P, *J*(PH) 12, *J*(HH) 12], 4.08 (s, 3 H, OMe), 7.11–7.68 (m, 20 H, Ph)	52.5 (s)
2	−19.25 [t, 1 H, μ-H, *J*(PH) 2], 0.89–2.63 [m, 10 H, $P(CH_2)_5P$], 4.02 (s, 3 H, OMe), 7.40–7.69 (m, 20 H, Ph)	55.4 (s)

[a] Measured in dichloromethane solution. [b] Based on ruthenium reactant. [c] Calculated values given in parentheses. [d] Chemical shifts (δ) in ppm, coupling constants in Hz. [e] Measured in [$^2H_2$]dichloromethane solution. [f] Hydrogen-1 decoupled. Chemical shifts positive to high frequency of 85% aqueous H_3PO_4 (external).

bidentate ligands. We wished to study the Au_2Ru_3 system further by preparing analogous clusters in which the two monodentate PPh_3 groups attached to the gold atoms are formally replaced by the bidentate diphosphine ligands $Ph_2P(CH_2)_nPPh_2$ (*n* = 1 or 5). The type of metal framework structure adopted by each of the new clusters was of interest. Our interest in preparing clusters analogous to $[Au_2Ru_3(\mu\text{-}H)(\mu_3\text{-}COMe)(CO)_9(PPh_3)_2]$ was also stimulated by a re-examination of some low-temperature ^{1}H NMR spectroscopic data[19] previously obtained for the clusters $[Au_2Ru_4(\mu\text{-}H)(\mu_3\text{-}H)(\mu\text{-}Ph_2ECH_2E'Ph_2)(CO)_{12}]$ (E = E′ = As or P; E = As, E′ = P).[9,10] In the spectrum of each compound a single signal for the methylene protons of the bidentate ligand attached to the gold atoms is observed at −90 °C, despite the fact that there is no plane of symmetry through the two Au atoms in the capped square-based pyramidal metal skeleton adopted by the clusters (see gold arrangement B in Fig. 1). It seems very unlikely that the peaks due to the expected two methylene proton environments would coincidentally have the same chemical shift for each of the three clusters. Therefore, it would seem that some fluxional process renders the two methylene hydrogen environments in each cluster equivalent on the NMR time-scale at −90 °C in solution. One possible mechanism for such a fluxional process is a rearrangement of the actual metal framework of the clusters. Although dynamic behaviour involving intramolecular metal core rearrangements is commonly observed for heteronuclear clusters containing two or more $Au(ER_3)$ units,[2,3,20] stereochemical non-rigidity of a metal framework with the gold atoms in arrangement B (Fig. 1) has not been previously reported. Unfortunately, it is not possible to use NMR spectroscopy to determine whether the Au_2Ru_3 metal skeleton of $[Au_2Ru_3(\mu\text{-}H)(\mu_3\text{-}COMe)(CO)_9(PPh_3)_2]$ undergoes similar dynamic behaviour. Although a ^{13}C-{^{1}H} NMR spectrum consistent with the ground-state structure is obtained at −60 °C, the broadening and coalescence observed for the carbonyl carbon signals as the temperature is raised[17] could also be due to intramolecular carbonyl ligand site exchange, which is a well established process for transition-metal organometallic clusters.[21] Therefore, we wished to prepare clusters analogous to $[Au_2Ru_3(\mu\text{-}H)(\mu\text{-}COMe)(CO)_9(PPh_3)_2]$ containing phosphine ligands with suitable ‘handles’ for variable-temperature NMR spectroscopic studies.

Results and Discussion

Synthesis and spectroscopic characterization of the new gold heteronuclear clusters $[Au_2Ru_3(\mu\text{-}H)(\mu_3\text{-}COMe)\{\mu\text{-}Ph_2P(CH_2)_nPPh_2\}(CO)_9]$ [*n* = 1 (1) or 5 (2)]

Treatment of a diethyl ether solution of the cluster compound $[Ru_3(\mu\text{-}H)_3(\mu_3\text{-}COMe)(CO)_9]$[22] with the complex $[Au_2\{\mu\text{-}Ph_2P(CH)_nPPh_2\}Me_2]$ (*n* = 1 or 5) affords the new mixed-metal cluster compounds $[Au_2Ru_3(\mu\text{-}H)(\mu_3\text{-}COMe)\{\mu\text{-}Ph_2P(CH_2)_nPPh_2\}(CO)_9]$ (*n* = 1 **1** or 5 **2**) in *ca.* 30–40% yield. Compounds **1** and **2** have been fully characterized by microanalysis and IR and NMR spectroscopy (Tables 1 and 2). The IR spectra of **1** and **2** are both closely similar to that previously reported for the analogous PPh_3-containing cluster $[Au_2Ru_3(\mu\text{-}H)(\mu_3\text{-}COMe)(CO)_9(PPh_3)_2]$ **3**, which suggests that **1** and **2** both adopt similar square-based pyramidal skeletal geometries, with the gold atoms in arrangement B (Fig. 1), to that established for **3**.[17] The ^{1}H and ^{31}P-{^{1}H} NMR spectra of **1** and **2** are also fully consistent with the formulations and the proposed metal core structure.

It is interesting that compounds **1** and **2** were the only products observed from the reactions between $[Ru_3(\mu\text{-}H)_3(\mu_3\text{-}COMe)(CO)_9]$ and the appropriate gold complex $[Au_2\{\mu\text{-}Ph_2P(CH_2)_nPPh_2\}Me_2]$. When $[Ru_3(\mu\text{-}H)_3(\mu_3\text{-}COMe)(CO)_9]$ was treated with $[AuMe(PPh_3)]$ two other products, $[AuRu_3(\mu\text{-}H)_2(\mu_3\text{-}COMe)(CO)_9(PPh_3)]$ and $[Au_3Ru_3(\mu_3\text{-}COMe)(CO)_9(PPh_3)_3]$, were obtained as well as $[Au_2Ru_3(\mu\text{-}H)(\mu_3\text{-}COMe)(CO)_9(PPh_3)_2]$ **3**.[16] However, no evidence for the formation of the linked clusters $[\{AuRu_3(\mu\text{-}H)_2(\mu_3\text{-}COMe)(CO)_9\}_2\{\mu\text{-}Ph_2P(CH_2)_nPPh_2\}]$ or $[\{Au_3Ru_3(\mu_3\text{-}COMe)(CO)_9\}_2\{\mu\text{-}Ph_2P(CH_2)_nPPh_2\}]$ (*n* = 1 or 5) was found during the syntheses of **1** and **2**, despite the fact that examples of gold heteronuclear clusters linked together by an $Au\{\mu\text{-}Ph_2P(CH_2)_nPPh_2\}Au$ unit have been reported previously.[23,24]

Crystal structures of the clusters $[Au_2Ru_3(\mu\text{-}H)(\mu_3\text{-}COMe)\{\mu\text{-}Ph_2P(CH_2)_nPPh_2\}(CO)_9]$ [*n* = 1 (1) or 5 (2)]

To investigate the structures of compounds **1** and **2** in detail, single-crystal X-ray diffraction studies were performed on both clusters. The molecular structures are shown in Figs. 2 and 3, respectively, and selected bond lengths and angles are summarized in Tables 3 and 4, respectively.

The structures are consistent with those deduced from the spectroscopic data. The metal cores of compounds **1** and **2** both adopt similar distorted square-based pyramidal structures. The square base of the pyramid is defined by the two Au atoms and two of the three Ru atoms [Ru(1)Ru(2)] with Ru(3) forming the apex of the pyramid. The bidentate diphosphine ligand $Ph_2P(CH_2)_nPPh_2$ (*n* = 1 or 5) bridges the two Au atoms, the methoxycarbyne group caps the Ru(1)Ru(2)Ru(3) face the hydride ligand bridges the basal Ru(1)–Ru(2) edge of the metal framework. Each ruthenium atom is also bonded to three

Table 2 Selected variable-temperature NMR spectroscopic data[a] used for the study of the dynamic behaviour of the clusters [Au$_2$Ru$_3$(μ-H)(μ$_3$-COMe){μ-Ph$_2$P(CH$_2$)$_n$PPh$_2$}(CO)$_9$] (n = 1 **1** or 5 **2**) in solution

(*a*) ^{1}H NMR[b]

Cluster	Temperature (°C)	Methylene proton and hydride ligand signals
1	−10	−18.57 [t, 1 H, μ-H, *J*(PH) 1], 3.21 [d of t, 1 H, PCH$_2$P, *J*(PH) 12, *J*(HH) 14], 3.37 [overlapping d of t, 1 H, PCH$_2$P, *J*(PH) 10, *J*(HH) 14]
	+80	−18.56 [t, 1 H, μ-H, *J*(PH) 1], 3.38 [t, 2 H, PCH$_2$P, *J*(PH) 11]
2	−20	−18.97 [t, 1 H, μ-H, *J*(PH) 2][c]
	+100	−18.84 [t, 1 H, μ-H, *J*(PH) 2], 1.33–1.44 [m, 4 H, P(CH$_2$)$_5$P], 2.01–2.05 [m, 2 H, P(CH$_2$)$_5$P], 2.35–2.40 [m, 4 H, P(CH$_2$)$_5$P]

(*b*) ^{31}P-{^{1}H} NMR[d]

		Signal
1	−90	51.1 (s)
2	−90	54.1 (s)

(*c*) ^{13}C-{^{1}H} NMR[e]

Cluster		Selected phenyl carbon signals[f]
1	−20	133.7 [AA′X pattern, C^2(Ph), *N*(PC) 21], 132.5 [AA′X pattern, C^2(Ph), *N*(PC) 20], 131.3 [s, C^4(Ph)], 131.2 [s, C^4(Ph)], 129.2 [AA′X pattern, C^3(Ph), *N*(PC) 14], 128.6 [AA′X pattern, C^3(Ph), *N*(PC) 13]
	+60	*ca.* 133 [s, vbr, C^2(Ph)], 131.0 [s, C^{4}Ph)], 128.8 [s, br, C^3(Ph)]
2	−20	133.8 [d, C^2(Ph), *J*(PC) 15], 133.6 [d, C^1(Ph), *J*(PC) 43], 133.2 [half of C^1(Ph) doublet with the other half obscured by the adjacent C^2(Ph) peak], 132.8 [d, C^2(Ph), *J*(PC) 13], 131.0 [s, C^4(Ph)], 130.8 [s, C^4(Ph)], 129.0 [d, C^3(Ph), *J*(PC) 11], 128.8 [d, C^3(Ph), *J*(PC) 10]
	+60	134.0 [d, C^1(Ph), *J*(PC) 42], 133.1 [d, C^2(Ph), *J*(PC) 14], 130.5 [d, C^4(Ph), *J*(PC) 2], 128.7 [d, C^3(Ph), *J*(PC) 10]

[a] Chemical shifts (δ) in ppm, coupling constants in Hz. [b] Measured in [^{2}H$_8$]toluene solution. [c] The methylene proton signals at this temperature have been omitted because they give no useful information about the dynamic behaviour of compound **2**. [d] Measured in [^{2}H$_2$]dichloromethane solution. Hydrogen-1 decoupled. Chemical shifts positive to high frequency of 85% aqueous H$_3$PO$_4$ (external). [e] Measured in [^{2}H$_8$]tetrahydrofuran solution. Hydrogen-1 decoupled. *N*(PC) = |*J*(PC) + *J*(P′C)|. [f] For cluster **1** the C^2(Ph), C^3(Ph) and C^4(Ph) signals were used for band-shape analysis, whereas only the C^2(Ph) and C^3(Ph) peaks were simulated for **2**.

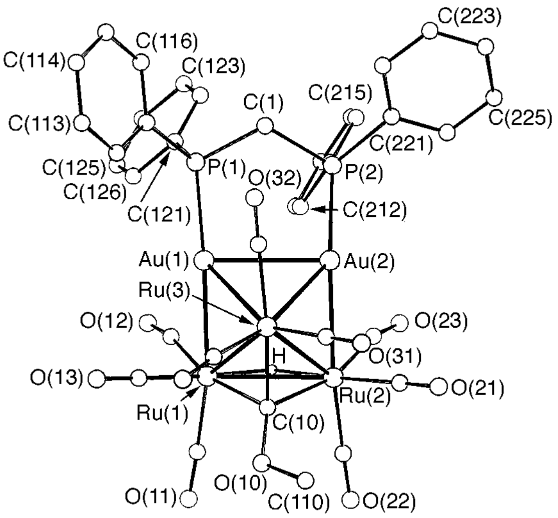

Fig. 2 Molecular structure of the cluster [Au$_2$Ru$_3$(μ-H)(μ$_3$-COMe)(μ-Ph$_2$PCH$_2$PPh$_2$)(CO)$_9$] **1**, showing the crystallographic numbering. The carbon atom of each carbonyl group has the same number as that of the oxygen atom

essentially linear CO groups. The overall metal core geometries of **1** and **2** are similar to that previously established for the PPh$_3$-containing analogue **3**. Fig. 4 compares the equivalent metal–metal separations in **1**, **2** and **3**.

The Au–Au distance in compound **1** [2.878(1) Å] is significantly shorter than that in **2** [3.109(1) Å], which reflects the greater stereochemical demands of the Ph$_2$PCH$_2$PPh$_2$ ligand in **1** compared with the Ph$_2$P(CH$_2$)$_5$PPh$_2$ ligand in **2**. As expected, the formal replacement of two PPh$_3$ ligands bonded to the gold atoms in **3** by the bidentate diphosphines Ph$_2$P(CH$_2$)$_n$PPh$_2$ (n = 1 or 5) in **1** and **2** causes a considerable reduction of the rather long Au–Au distance of 3.176(1) Å (Fig. 4) and the magnitude of this decrease is greater for **1** (*ca.* 0.298 Å) than for **2** (*ca.* 0.066 Å).

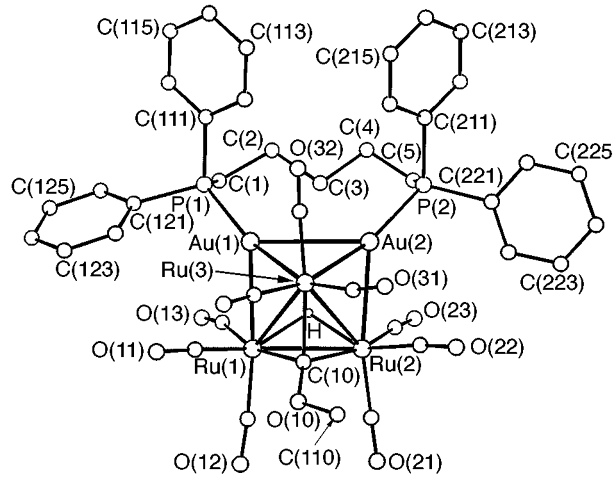

Fig. 3 Molecular structure of the cluster [Au$_2$Ru$_3$(μ-H)(μ$_3$-COMe){μ-Ph$_2$P(CH$_2$)$_5$PPh$_2$}(CO)$_9$] **2**. Details as in Fig. 2

The ranges of Au–Ru distances in compounds **1**, **2** and **3** (Fig. 4) are similar, but the mean in the PPh$_3$-containing cluster **3** [2.746(1) Å] is *ca.* 0.010 Å shorter than that in **2** [2.756(2) Å] and *ca.* 0.021 Å shorter than that in **1**. In contrast, there is a much smaller variation in the Ru–Ru distances with the mean in cluster **3** [2.879(2) Å] being *ca.* 0.010 Å shorter than that in **1** [2.889(1) Å] and *ca.* 0.003 Å shorter than that in **2** [2.882(2) Å]. Changes in the nature of the ligand(s) attached to the gold atoms in **1**–**3** have a much greater effect on the values of the Au–Ru separations than on the magnitudes of the Ru–Ru separations, as has been previously observed for gold heteronuclear clusters.[2,3] However, it is interesting that the Ph$_2$PCH$_2$PPh$_2$ ligand causes an increase of *ca.* 0.029 Å in the length of the Ru(1)–Ru(2) vector in **1** when it formally replaces either Ph$_2$P(CH$_2$)$_5$PPh$_2$ in **2** or two PPh$_3$ groups in **3**. This change is considerably larger than those observed for the other Ru–Ru

Table 3 Selected bond lengths (Å) and angles (°), with estimated standard deviations (e.s.d.s) in parentheses for [Au_2Ru_3(μ-H)-($μ_3$-COMe)(μ-$Ph_2PCH_2PPh_2$)$(CO)_9$] **1**

Au(1)–Au(2)	2.8777(7)	Au(1)–Ru(1)	2.6883(10)
Au(1)–Ru(3)	2.8631(10)	Au(1)–P(1)	2.313(3)
Au(1) · · · Ru(2)	4.01(3)	Au(2) · · · Ru(1)	3.90(3)
Au(2)–Ru(2)	2.7205(10)	Au(2)–Ru(3)	2.7947(11)
Au(2)–P(2)	2.316(3)	Ru(1)–Ru(2)	2.889(2)
Ru(1)–Ru(3)	2.8873(13)	Ru(2)–Ru(3)	2.8913(14)
Ru(1)–C(10)	2.064(10)	Ru(2)–C(10)	2.088(1)
Ru(3)–C(10)	2.052(10)		
Ru–CO range	1.854(13)–1.950(14)		
C–O range	1.13(2)–1.20(2)		

Ru(1)–Au(1)–Au(2)	88.87(3)	Ru(3)–Au(1)–Au(2)	58.26(2)
Ru(1)–Au(1)–Ru(3)	62.59(3)	P(1)–Au(1)–Au(2)	95.05(7)
P(1)–Au(1)–Ru(1)	161.38(8)	P(1)–Au(1)–Ru(3)	134.19(7)
Ru(2)–Au(2)–Au(1)	91.35(3)	Ru(3)–Au(2)–Au(1)	60.61(2)
P(2)–Au(2)–Ru(2)	153.39(8)	P(2)–Au(2)–Ru(3)	138.66(8)
Ru(2)–Au(2)–Ru(3)	63.22(3)	P(2)–Au(2)–Au(1)	90.88(7)
Au(1)–Ru(1)–Ru(3)	61.67(3)	Au(1)–Ru(1)–Ru(2)	91.76(3)
Ru(3)–Ru(1)–Ru(2)	60.07(3)	Au(2)–Ru(2)–Ru(1)	88.02(4)
Au(2)–Ru(2)–Ru(3)	59.64(3)	Ru(1)–Ru(2)–Ru(3)	59.93(3)
Au(2)–Ru(3)–Au(1)	61.13(2)	Au(2)–Ru(3)–Ru(1)	86.65(3)
Au(1)–Ru(3)–Ru(1)	55.74(3)	Au(2)–Ru(3)–Ru(2)	57.14(3)
Au(1)–Ru(3)–Ru(2)	88.25(3)	Ru(1)–Ru(3)–Ru(2)	59.99(3)
C(1)–+(1)–Au(1)	109.7(4)	C(1)–P(2)–Au(2)	110.1(4)
Ru–C–O range	164(2)–179(2)		

Table 4 Selected bond lengths (Å) and angles (°), with e.s.d.s in parentheses, for [Au_2Ru_3(μ-H)($μ_3$-COMe){μ-$Ph_2P(CH_2)_5PPh_2$}$(CO)_9$] **2**

Au(1)–Au(2)	3.109(1)	Au(1)–Ru(1)	2.787(3)
Au(1)–Ru(3)	2.716(2)	Au(1)–P(1)	2.321(7)
Au(1) · · · Ru(2)	4.05(3)	Au(2) · · · Ru(1)	3.95(3)
Au(2)–Ru(2)	2.785(3)	Au(2)–Ru(3)	2.734(2)
Au(2)–P(2)	2.304(7)	Ru(1)–Ru(2)	2.859(2)
Ru(1)–Ru(3)	2.895(3)	Ru(2)–Ru(3)	2.892(3)
Ru(1)–C(10)	2.015(19)	Ru(2)–C(10)	2.067(19)
Ru(3)–C(10)	2.062(25)		
Ru–CO range	1.777(22)–1.945(23)		
C–O range	1.14(3)–1.20(3)		

Ru(1)–Au(1)–Au(2)	88.4(1)	Ru(3)–Au(1)–Au(2)	55.5(1)
Ru(3)–Au(1)–Ru(1)	63.5(1)	P(1)–Au(1)–Au(2)	123.3(2)
P(1)–Au(1)–Ru(1)	133.6(2)	P(1)–Au(1)–Ru(3)	161.6(2)
Ru(2)–Au(2)–Au(1)	86.5(1)	Ru(3)–Au(2)–Au(1)	54.9(1)
Ru(3)–Au(2)–Ru(2)	63.2(1)	P(2)–Au(2)–Au(1)	125.6(2)
P(2)–Au(2)–Ru(2)	134.1(2)	P(2)–Au(2)–Ru(3)	160.5(2)
Ru(2)–Ru(1)–Au(1)	91.5(1)	Ru(3)–Ru(1)–Au(1)	57.1(1)
Ru(3)–Ru(1)–Ru(2)	60.3(1)	Ru(1)–Ru(2)–Au(2)	93.6(1)
Ru(3)–Ru(2)–Au(2)	57.5(1)	Ru(3)–Ru(2)–Ru(1)	60.5(1)
Au(2)–Ru(3)–Au(1)	69.6(1)	Ru(1)–Ru(3)–Au(1)	59.4(1)
Ru(1)–Ru(3)–Au(2)	93.9(1)	Ru(2)–Ru(3)–Au(1)	92.3(1)
Ru(2)–Ru(3)–Au(2)	59.3(1)	Ru(2)–Ru(3)–Ru(1)	59.2(1)
C(1)–P(1)–Au(1)	116.7(9)	C(5)–P(2)–Au(2)	114.3(9)
Ru–C–O range	165(2)–179(2)		

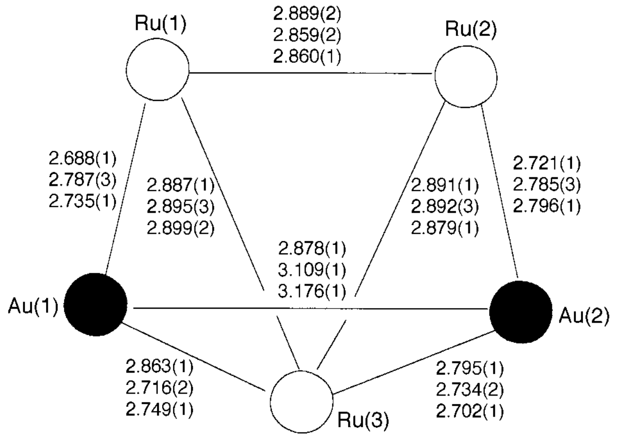

Fig. 4 Comparison of the equivalent metal–metal separations (Å) in the metal frameworks of [Au_2Ru_3(μ-H)($μ_3$-COMe){μ-$Ph_2P(CH_2)_nPPh_2$}$(CO)_9$] (*n* = 1 **1** or 5 **2**) and [Au_2Ru_3(μ-H)($μ_3$-COMe)$(CO)_9(PPh_3)_2$] **3**. Distances are given in the following descending order: **1**, **2** and **3**[17]

separations within **1**–**3**. The bases of the square-based pyramidal metal frameworks in all three structures exhibit a similar degree of distortion [Au(1) · · · Ru(2) 4.01(3) and Au(2) · · · Ru(1) 3.90(3) in **1**; Au(1) · · · Ru(2) 4.05(3) and Au(2) · · · Ru(1) 3.95(3) in **2**; Au(1) · · · Ru(2) 4.03(3) and Au(2) · · · Ru(1) 3.98(3) Å in **3**]. The capping methoxycarbyne ligand in each of **1** and **2** caps the Ru_3 face asymmetrically, which is similar to the bonding mode previously established for cluster **3**.[17]

It was anticipated that, with the increase in the length of the methylene backbone in the diphosphine ligand in cluster **2**, a greater degree of freedom would be available for the $Ph_2P(CH_2)_5PPh_2$ group to adopt a sterically favourable edge-bridging configuration on the metal core. Interestingly, the X-ray data show the opposite trend. Within experimental error, the mean Au–P distances in **1** and **2** are similar [2.315(3) for **1** and 2.313(7) Å for **2**]. However, evidence of strain within the Au–P–C ring system in cluster **2** relative to its $Ph_2PCH_2PPh_2$-containing analogue **1** is evident when the respective Au–P–C angles are compared. The mean Au–P–C intercyclic angle in **1** [110(2)°] is near to the ideal tetrahedral angle, whereas in **2** this angle becomes distorted to a larger value [115(3)°]. Similar observation of induced conformational strain with increases in chain length in diphosphine ligands have also recently been reported for the hexaruthenium cluster series [Ru_6C{μ-$Ph_2P(CH_2)_nPPh_2$}$(CO)_{15}$] (*n* = 1–3).[25]

In each of compounds **1** and **2** there are several short contact distances between the gold atoms and carbon atoms of the CO ligands; three in cluster **1**, Au(1) · · · C(12) 2.661(14), Au(1) · · · C(32) 2.693(13) and Au(2) · · · C(23) 2.641(12) Å, and two in **2**, Au(1) · · · C(13) 2.67(3) and Au(1) · · · C(32) 2.651(22) Å. This structural feature is present in many Group IB metal heteronuclear clusters, but it is not well understood and it is not clear whether the contacts represent some degree of long-range interactions, either attractive or repulsive, between the coinage metals and the CO ligands or result from steric effects in the solid state.[2,3]

Variable-temperature NMR spectroscopic studies on the clusters [Au_2Ru_3(μ-H)($μ_3$-COMe){μ-$Ph_2P(CH_2)_nPPh_2$}$(CO)_9$] [*n* = 1 (1) or 5 (2)]

The peaks due to the methylene hydrogens in the ^1H NMR spectrum of compound **1** at −10 °C consist of two doublets of triplets (Table 2), which is consistent with the ground-state structure of the cluster in which the two methylene hydrogens are inequivalent (Fig. 5). However, as the temperature is raised from −10 °C, the two separate methylene hydrogen signals broaden and then coalesce, until at +80 °C a triplet with narrow linewidths is observed (Table 2). Therefore, at +80 °C in solution, cluster **1** must undergo a fluxional process which renders the two methylene hydrogen atoms equivalent on the NMR time-scale. The signal due to the hydride ligand is split into a triplet by ^{31}P–^1H coupling at −10 and also at +80 °C (Table 2), so the fluxional process occurring cannot be intermolecular. The variable-temperature spectra can be explained by either of two different intramolecular fluxional processes. The two phosphorus atoms of the bidentate diphosphine ligand $Ph_2PCH_2PPh_2$ could be undergoing intramolecular site exchange between the two gold atoms in the Au_2Ru_3 metal core of **1** or the actual metal skeleton of the cluster could itself be stereochemically non-rigid in solution. Although dynamic behaviour involving intramolecular site exchange of the two phosphorus atoms in the bidentate diphosphine ligand *cis*-Ph_2PCH=$CHPPh_2$ between the two silver atoms has been previously observed in solution for the cluster [$Ag_2Ru_4(μ_3\text{-}H)_2$(μ-*cis*-

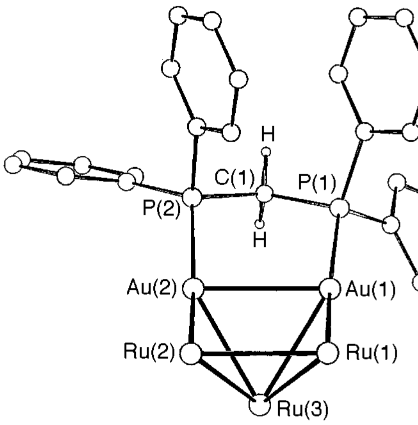

Fig. 5 The metal core of the cluster $[Au_2Ru_3(\mu-H)(\mu_3-COMe)(\mu-Ph_2PCH_2PPh_2)(CO)_9]$ **1**, showing the two inequivalent methylene proton environments and the inequivalence of the two phenyl rings attached to each phosphorus atom in the ground-state structure. The carbonyl, hydride and methoxycarbyne ligands have been omitted for clarity

$Ph_2PCH{=}CHPPh_2)(CO)_{12}]$,[12] the $Ph_2P(CH_2)_4PPh_2$ ligand in the analogous cluster $[Ag_2Ru_4(\mu_3-H)_2\{\mu-Ph_2P(CH_2)_4PPh_2\}(CO)_{12}]$ did not exhibit similar fluxionality on the NMR time-scale, even at +100 °C.[12] Furthermore, no examples of the phosphorus atoms in bidentate diphosphine ligands undergoing intramolecular site exchange between gold atoms in heteronuclear clusters have been reported previously[2,3] and low-energy processes involving intramolecular site exchange for phosphine ligands are extremely rare for cluster compounds in general.[12] However, the metal frameworks of Group IB metal heteronuclear clusters are often observed to be stereochemically non-rigid on the NMR time-scale in solution.[2,3,7,20] Therefore, an intramolecular metal core rearrangement of the square-based pyramidal Au_2Ru_3 skeleton of **1** seems to be a very much more likely explanation for the observed variable-temperature ^1H NMR spectroscopic results than a fluxional process involving intramolecular site exchange of the phosphorus atoms in $Ph_2PCH_2PPh_2$, although the latter process cannot be completely ruled out on the evidence available. The proposed mechanism for the rearrangement of the metal core of **1** involves a migration of the diphosphinedigold unit around the three edge-bridging Ru–Ru sites of the trigonal-planar Ru_3 moiety (Fig. 6) and it can be viewed as a rotation of the diphosphinedigold unit around the centre of the Ru_3 triangle. The proposed dynamic behaviour of the metal core of **1** creates an effective mirror plane through the $Ph_2PCH_2PPh_2$ ligand, which is attached to the two gold atoms, and hence renders the two methylene hydrogens equivalent on the NMR time-scale. The rearrangement of the Au_2Ru_3 metal skeleton must be accompanied by a concomitant migration of the hydride ligand around the Ru–Ru edges of the trigonal-planar Ru_3 fragment. It is interesting that the edge-bridging $Au(PPh_3)$ unit in the cluster $[AuRu_3\{\mu_3-(Me_2P)_3CH\}(CO)_9(PPh_3)][O_3SCF_3]$ is known to undergo migration around the three edges of the trigonal-planar Ru_3 unit in solution.[26] This fluxional process is fast on the NMR time-scale at ambient temperatures, but a $^{31}P-\{^1H\}$ NMR spectrum consistent with the ground-state structure of the cluster was obtained at low temperatures.

The variable-temperature ^1H NMR spectra of compound **2** are consistent with the Au_2Ru_3 metal core of this cluster also undergoing a similar intramolecular rearrangement process to that proposed for **1**. At −90 °C the peaks due to the methylene hydrogens are a very complex ten-proton multiplet. Such a very complex multiplet would be expected from the ground-state structure of **2**, in which there are six distinct environments for the methylene hydrogens (Fig. 3). As the temperature is raised, broadening and some coalescence occurs for the methylene hydrogen multiplet, until eventually at +100 °C two four-proton multiplets and a two-proton multiplet, with relatively narrow linewidths (Table 2), are observed. The peaks visible at the high-temperature limit are consistent with the pair of inequivalent hydrogens on each methylene carbon being rendered equivalent by a fluxional process. Again, $^{31}P-^1H$ coupling is observed for the hydride ligand signal of **2** at the high- and low-temperature limits (Table 2), so an intermolecular fluxional process can be ruled out.

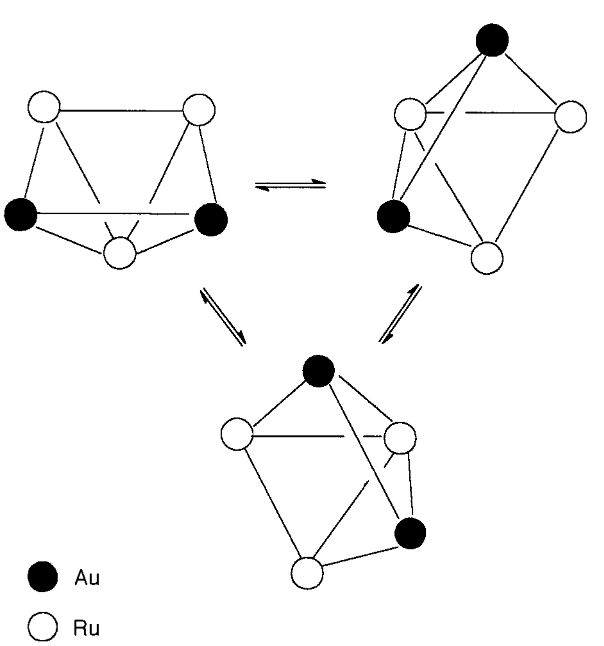

Fig. 6 Mechanism proposed for the intramolecular metal core rearrangement of the square-based pyramidal metal skeletons of the clusters $[Au_2Ru_3(\mu-H)(\mu_3-COMe)\{\mu-Ph_2P(CH_2)_nPPh_2\}(CO)_9]$ ($n = 1$ **1** or 5 **2**). The fluxional process creates an effective mirror plane through the $Ph_2P(CH_2)_nPPh_2$ ligand, which is attached to the two gold atoms, and hence renders the pair of hydrogens on each methylene carbon equivalent on the NMR time-scale

It is of interest to determine and compare the free energies of activation ($\Delta G^\ddagger$) for the proposed intramolecular metal core rearrangements in clusters **1** and **2**. Band-shape analysis of the methylene proton signals in the variable-temperature ^1H NMR spectra of **1** readily affords the values of the thermodynamic parameters for the fluxional process in **1** (Table 5), but the methylene proton signals for **2** are too complicated to allow similar treatment (Table 2). However, the dynamic behaviour of **1** and **2** can also be studied by variable-temperature $^{13}C-\{^1H\}$ NMR spectroscopy. In each case, at the low-temperature limit, two sets of signals are observed for the phenyl carbons of the bidentate diphosphine ligand, but these peaks broaden and coalesce into a single set of phenyl carbon signals as the temperature is raised (Table 2). Band-shape analysis of selected (Table 2) phenyl carbon signals in the variable-temperature $^{13}C-\{^1H\}$ NMR spectra of **1** and **2** affords the thermodynamic parameters for the metal-core rearrangements of the clusters (Table 5).

It is well established that energies quoted in terms of $\Delta G^\ddagger$ values are less prone to systematic errors than the other parameters calculated by band-shape analysis and, therefore, $\Delta G^\ddagger$ values are normally used for comparison purposes.[27] Table 5 shows that the magnitude of $\Delta G^\ddagger$ for the metal-core rearrangement of **1** determined from ^1H NMR spectroscopy is identical within experimental error to that obtained from $^{13}C-\{^1H\}$ NMR spectroscopy. The value of $\Delta G^\ddagger$ for the metal-framework rearrangement in **2** is considerably lower (*ca.* 8 kJ mol^{-1}) than that observed for **1**. The difference may possibly be a reflection of the greater flexibility of the $(CH_2)_5$ backbone of the bidentate diphosphine in **2**.

The magnitude of $\Delta S^\ddagger$ for intramolecular processes in organometallic complexes are frequently found to be between

Table 5 Energy parameters[a] for the intramolecular metal-core rearrangement observed in solution for the clusters $[Au_2Ru_3(\mu\text{-}H)(\mu_3\text{-}COMe)\{\mu\text{-}Ph_2P(CH_2)_nPPh_2\}(CO)_9]$ (n = 1 **1** or 5 **2**)

Cluster	$\Delta G^‡$/kJ mol^{-1}	$\Delta S^‡$/J K^{-1} mol^{-1}	$\Delta H^‡$/kJ mol^{-1}
1	67.1 ± 0.2[b]	7.5 ± 10.5[b]	69.3 ± 3.3[b]
	67.0 ± 0.2	14.8 ± 15.2	71.4 ± 4.7
2	58.9 ± 0.1	−19.9 ± 11.1	52.9 ± 3.2

[a] Calculated at 298.15 K by band-shape analysis of selected (see Table 2) phenyl carbon signals in variable-temperature $^{13}C\text{-}\{^1H\}$ NMR spectra, unless otherwise stated. [b] Calculated at 298.15 K by band-shape analysis of the methylene hydrogen signals in variable-temperature ^1H NMR spectra.

+20 and −20 J K^{-1} mol^{-1} [28] and all of the $\Delta S^‡$ values calculated for **1** and **2** (Table 5) lie in this range. This observation is consistent with the proposed intramolecular nature of the fluxional processes which **1** and **2** undergo in solution.

Although many examples of gold-containing heteronuclear clusters which have metal skeletons that exhibit stereochemical non-rigidity have appeared in the literature,[2,3,20] to the best of our knowledge this paper contains the first specific report of an intramolecular metal-core rearrangement for a cluster with gold arrangement B (Fig. 1). However, a similar fluxional process to that postulated herein would also explain the single methylene proton environments observed in the low-temperature ^1H NMR spectra of each of the clusters $[Au_2Ru_4(\mu\text{-}H)(\mu_3\text{-}H)(\mu\text{-}Ph_2ECH_2E'Ph_2)(CO)_{12}]$ (E = E′ = As or P; E = As, E′ = P) (see introduction).[9,10,19] It is interesting that the proposed metal-core rearrangement in each of the above clusters must have a very much smaller value of $\Delta G^‡$ than those observed for **1** and **2**, since a ^1H NMR spectrum consistent with the ground-state structure could not be obtained for any of the hexanuclear clusters, even at −90 °C.[19] These very low $\Delta G^‡$ values also suggest that the fluxional process causing the equivalence of the methylene protons in the bidentate ligands is not an intramolecular site exchange of the E (As or P) atoms between the two gold atoms.

It is also interesting to examine the NMR spectroscopic data reported for the cluster $[Au_2Ru_6C(\mu\text{-}Ph_2PCH_2PPh_2)(CO)_{16}]$, which has a metal-framework structure consisting of a square-based pyramidal Au_2Ru_3 unit (gold arrangement B in Fig. 1) and an Ru_6 octahedron containing an interstitial carbide ligand fused together by sharing a common Ru_3 face. Although the two methylene hydrogens and the two phosphorus atoms in the $Ph_2PCH_2PPh_2$ ligand, which is attached to the two gold atoms, are both inequivalent in the ground-state structure, a triplet is reported for the methylene hydrogen signal in the ^1H NMR spectrum and a singlet[11] for the $^{31}P\text{-}\{^1H\}$ NMR spectrum. The authors do not comment on their NMR spectroscopic data, but an intramolecular metal-core rearrangement for the square-based pyramidal Au_2Ru_3 moiety in the octanuclear cluster similar to that observed for **1** and **2** (Fig. 5) would explain the apparent equivalence of the two methylene hydrogens and the two phosphorus atoms on the NMR time-scale in solution.

Experimental

All reactions were performed under an atmosphere of dry oxygen-free nitrogen, using Schlenk-tube techniques.[29] Solvents were freshly distilled under nitrogen from the usual drying agents immediately before use. Light petroleum refers to that fraction of b.p. 40–60 °C. Established methods were used to prepare the cluster $[Ru_3(\mu\text{-}H)_3(\mu_3\text{-}COMe)(CO)_9]$[22] and the compound $[AuCl(SC_4H_8)]$.[30] The bidentate diphosphines $Ph_2P(CH_2)_nPPh_2$ (n = 1 or 5) were purchased from Strem Chemicals Inc. and used without further purification. Methyllithium (a 1.4 M solution in diethyl ether) was supplied by Aldrich Chemical Co. Product separation was performed on BDH alumina (Brockman activity II). Infrared spectra were recorded on a Perkin-Elmer 881 spectrophotometer and NMR spectra on a Bruker DRX 400 spectrometer. Analytical, physical and IR and NMR spectroscopic data for the new gold heteronuclear cluster compounds are presented in Table 1.

Synthesis of the complexes $[Au_2\{\mu\text{-}Ph_2P(CH_2)_nPPh_2\}Me_2]$ (n = 1 or 5)

An adaptation of the standard literature procedure for the preparation of $[AuMe(PPh_3)]$[30] was utilized. A dichloromethane (80 cm^3) solution of the compound $[AuCl(SC_4H_8)]$ (0.94 g, 2.92 mmol) was treated with $Ph_2P(CH_2)_nPPh_2$ (n = 1, 0.56 g, 1.46 mmol; or n = 5, 0.58 g, 1.46 mmol). After stirring the reaction mixture for 10 min, the solvent was removed under reduced pressure and diethyl ether (200 cm^3) added to the residue which consisted of crude $[Au_2\{\mu\text{-}Ph_2P(CH_2)_nPPh_2\}Cl_2]$. The resulting suspension was cooled to −70 °C and treated with a 1.4 M solution of LiMe in diethyl ether (2.2 cm^3, 3.22 mmol). After the reaction mixture was allowed to warm to ambient temperature with stirring, water (0.6 cm^3) was added to destroy any unreacted LiMe. The reaction mixture was then filtered through a small pad of anhydrous magnesium sulfate (*ca.* 5 × 3 cm) and the solvent was removed under reduced pressure to afford the complex $[Au_2\{\mu\text{-}Ph_2P(CH_2)_nPPh_2\}Me_2]$ (n = 1 or 5). The crude samples of the gold complexes prepared in this manner were used for the syntheses of the heteronuclear clusters **1** and **2** without further purification.

Synthesis of the gold heteronuclear clusters $[Au_2Ru_3(\mu_3\text{-}COMe)\{\mu\text{-}Ph_2P(CH_2)_nPPh_2\}(CO)_9]$ [n = 1 (1) or 5 (2)]

A sample of the appropriate complex $[Au\{\mu\text{-}Ph_2P(CH_2)_n\text{-}PPh_2\}Me_2]$ (n = 1, 0.43 g, 0.54 mmol; or n = 5, 0.44 g, 0.56 mmol), prepared as described above, was added to a diethyl ether (150 cm^3) solution of $[Ru_3(\mu\text{-}H)_3(\mu_3\text{-}COMe)(CO)_9]$ (0.27 g, 0.45 mmol) and the mixture stirred for *ca.* 15 h. After removal of the solvent under reduced pressure, the residue was dissolved in dichloromethane–light petroleum (1 : 4) and chromatographed on an alumina (20 × 3 cm) column. Gradient elution with a dichloromethane–light petroleum mixture, initially 1 : 4 then increasing to 1 : 1 after recovery of the first band, allowed the separation of the unchanged yellow starting material $[Ru_3(\mu\text{-}H)_3(\mu_3\text{-}COMe)(CO)_9]$ and the orange gold-containing heteronuclear cluster. After removal of the solvent from the second, orange fraction under reduced pressure, crystallization of the residue from a dichloromethane–light petroleum mixture yielded orange *microcrystals* of the product $[Au_2Ru_3(\mu\text{-}H)(\mu_3\text{-}COMe)\{\mu\text{-}Ph_2P(CH_2)_nPPh_2\}(CO)_9]$ (n = 1, 0.17 g; or n = 5, 0.22 g).

Variable-temperature NMR spectroscopic studies

Variable-temperature NMR spectra of clusters **1** and **2** for computer simulation (see Table 2 for details) were recorded on a Bruker DRX 400 spectrometer operating at 400.13 and 100.62 MHz for the ^1H and ^{13}C nuclei, respectively. The solvents used were $[^2H_8]$toluene for the ^1H NMR spectra and $[^2H_8]$tetrahydrofuran for the $^{13}C\text{-}\{^1H\}$ NMR spectra. Samples were prepared under an atmosphere of dry, oxygen-free nitrogen in standard 5 mm NMR tubes. A standard Eurotherm B-VT2000 variable-temperature unit was used to control the probe temperature. The temperatures are considered accurate to ±1 °C.

Rate data were obtained from band-shape analysis of variable-temperature ^1H or $^{13}C\text{-}\{^1H\}$ NMR spectra using a modified version of the standard DNMR program[32] of Kleier and Binsch.[33] Activation parameters based on experimental rate data were calculated using the THERMO program.[32]

Crystallography

Suitable crystals of compounds **1** and **2** were grown from

Table 6 Crystal structure determination data for clusters $[Au_2Ru_3(\mu\text{-}H)(\mu_3\text{-}COMe)\{\mu\text{-}Ph_2P(CH_2)_nPPh_2\}(CO)_9]$ (n = 1 **1** or 5 **2**)

	1	**2**
Molecular formula	$C_{36}H_{26}Au_2O_{10}P_2Ru_3$	$C_{40}H_{34}Au_2O_{10}P_2Ru_3$
M	1377.65	1434.1
Crystal dimensions/mm	0.26 × 0.23 × 0.15	0.25 × 0.22 × 0.23
Crystal system	Triclinic	Monoclinic
Space group	$P\bar{1}$ (no. 2)	$P2_1/c$
a/Å	10.5383(13)	20.610(3)
b/Å	12.2503(10)	10.017(2)
c/Å	17.0412(12)	22.473(3)
α/°	72.274(4)	
β/°	79.003(7)	108.198(2)
γ/°	74.055(9)	
U/Å^3	2001.1	4407.5
D_c/g cm^{-3}	2.286	2.161
Z	2	4
F(000)	1284	2696
μ(Mo-Kα)/mm^{-1}	8.55	7.44
T/K	293	298
No. reflections measured	8239	8746
No. independent reflections (R_{int})	6989 (0.033)	7746 (0.045)[a]
No. of refined parameters	201	225
Goodness of fit on F^2	1.005	1.100
Refinement method	Full-matrix least squares on F^2	Full-matrix least squares on F
$R1$	0.0478[b]	0.0592[c]
(all data)	0.0856	—
$R' = \Sigma w^{\frac{1}{2}}(\|\|F_o\| - \|F_c\|\|)/\Sigma w^{\frac{1}{2}}\|F_o\|$	—	0.0584[c]
$wR2$	0.0872[b]	—
(all data)	0.1022	—
Largest difference peak and hole/e Å^{-3}	0.429, −0.370	0.32, −0.67

[a] 3288 with $I > 3\sigma(I)$. [b] $I > 2\sigma(I)$. [c] $I > 3\sigma(I)$.

dichloromethane–light petroleum solutions by slow layer diffusion at −20 °C.

Data collection. Details of crystal parameters, data collection parameters and refinement data are summarized in Table 6. Data for compound **1** were collected using a red crystal mounted on a quartz fibre on a Siemens P4 diffractometer in the range θ = 1.26–25° using Mo-Kα graphite-monochromated radiation (λ = 0.710 73 Å). Data collection for **2** was carried out using a red crystal mounted on a quartz fibre on a Philips PW1100 diffractometer in the range θ = 3–25° with graphite-monochromated Mo-Kα radiation (λ = 0.710 69 Å).

Structure solution and refinement. *Compound* **1.**[34] The structure was solved by direct methods and subsequent Fourier-difference syntheses revealed the position of all of the non-hydrogen atoms. Although the hydride ligand was not located directly from the data, a suitable position was obtained from potential-energy minimization calculations,[35] which was included in the structure-factor calculations with a fixed thermal parameter of 0.075 Å^2. The carbon atoms of the phenyl rings were grouped together as rigid hexagons [d(C–C) = 1.395 Å] and their hydrogen atoms, together with those of the methyl and methylene carbon atoms, were included in geometrically idealized positions and constrained to 'ride' on the relevant carbon atoms [d(C–H) = 0.98 Å] with common group isotropic thermal parameters of 0.075 Å^2, which were not refined. Data were corrected for absorption using semiempirical ψ scans (T_{max} 0.384, T_{min} 0.106). Anisotropic thermal parameters were assigned to the metal and the phosphorus atoms during the final cycles of full-matrix refinement with weights of $[\sigma^2(F_o^2) + (0.0333P)^2 + 14.2572]^{-1}$, where $P = [\max(F_o^2, 0) + 2F_c^2]/3$, assigned to individual reflections.

Compound **2.**[36] The positions of the metal atoms were deduced from a Patterson synthesis. A series of Fourier-difference syntheses revealed the positions of all the remaining non-hydrogen atoms. Although the hydride ligand was not located directly, a suitable position was obtained as above[34] and included in the structure-factor calculations with a fixed thermal parameter of 0.08 Å^2. The carbon atoms of phenyl rings were treated as above and their hydrogen atoms, together with those of the methyl and methylene carbon atoms, constrained to 'ride' on the relevant carbon atoms [d(C–H) = 1.08 Å] with common group isotropic thermal parameters of 0.08 Å^2, which were not refined. After isotropic refinement of all of the non-hydrogen atoms, an empirical absorption correction[37] was applied (T_{max} 1.023, T_{min} 0.866). In the final cycles of full-matrix least-squares refinement individual weights of $1/\sigma^2(F_o)$ were assigned to each reflection and anisotropic thermal parameters were assigned to the metal and the phosphorus atoms.

CCDC reference number 186/853.

Acknowledgements

We would like to thank Dr Keith Orrell for suggesting the use of variable-temperature $^{13}C\text{-}\{^1H\}$ NMR spectroscopy to obtain values of the thermodynamic parameters for the metal-core rearrangements, the University of Exeter Research Fund for supporting this work (C. A. C. and S. A. W.) and Johnson Matthey plc for a generous loan of gold and ruthenium starting materials.

References

1 Part 20, I. D. Salter, V. Šik, S. A. Williams and T. Adatia, *J. Chem. Soc., Dalton Trans.*, 1996, 643.
2 I. D. Salter, in *Comprehensive Organometallic Chemistry II*, eds. G. Wilkinson, F. G. A. Stone and E. W. Abel, Pergamon, Oxford, 1995, vol. 10, p. 255.
3 I. D. Salter, *Adv. Organomet. Chem.*, 1989, **29**, 249.
4 D. M. P. Mingos, *Polyhedron*, 1984, **3**, 1289.
5 D. G. Evans and D. M. P. Mingos, *J. Organomet. Chem.*, 1982, **232**, 171.
6 K. P. Hall and D. M. P. Mingos, *Prog. Inorg. Chem.*, 1984, **32**, 327.
7 D. M. P. Mingos and M. J. Watson, *Adv. Inorg. Chem.*, 1992, **39**, 327.
8 S. S. D. Brown, S. Hudson, I. D. Salter and M. McPartlin, *J. Chem. Soc., Dalton Trans.*, 1987, 1967.

9 S. S. D. Brown, I. D. Salter, A. J. Dent, G. F. M. Kitchen, A. G. Orpen, P. A. Bates and M. B. Hursthouse, *J. Chem. Soc.*, *Dalton Trans.*, 1989, 1227.

10 S. S. D. Brown, I. D. Salter, D. B. Dyson, R. V. Parish, P. A. Bates and M. B. Hursthouse, *J. Chem. Soc.*, *Dalton Trans.*, 1988, 1795.

11 P. J. Bailey, M. A. Beswick, J. Lewis, P. R. Raithby and M. Carmen Ramizez de Arellano, *J. Organomet. Chem.*, 1993, **459**, 293.

12 C. P. Blaxill, S. S. D. Brown, J. C. Frankland, I. D. Salter and V. Šik, *J. Chem. Soc.*, *Dalton Trans.*, 1989, 2039.

13 T. Adatia, *Acta Crystallogr.*, *Sect. C*, 1993, **49**, 1926.

14 M. J. Freeman, A. G. Orpen and I. D. Salter, *J. Chem. Soc.*, *Dalton Trans.*, 1987, 379.

15 S. R. Bunkhall, H. D. Holden, B. F. G. Johnson, J. Lewis, G. N. Pain, P. R. Raithby and M. J. Taylor, *J. Chem. Soc.*, *Chem. Commun.*, 1984, 25.

16 L. W. Bateman, M. Green, K. A. Mead, R. M. Mills, I. D. Salter, F. G. A. Stone and P. Woodward, *J. Chem. Soc.*, *Dalton Trans.*, 1983, 2599.

17 L. J. Farrugia, M. J. Freeman, M. Green, A. G. Orpen, F. G. A. Stone and I. D. Salter, *J. Organomet. Chem.*, 1983, **249**, 273.

18 C. M. Hay, B. F. G. Johnson, J. Lewis, R. C. S. McQueen, P. R. Raithby, R. M. Sorrell and M. J. Taylor, *Organometallics*, 1985, **4**, 202.

19 S. S. D. Brown and I. D. Salter, unpublished work.

20 I. D. Salter, *Adv. Dynamic Stereochem.*, 1988, **2**, 57.

21 See, for example, B. F. G. Johnson and R. E. Benfield, in *Transition Metal Clusters*, ed. B. F. G. Johnson, Wiley, New York, 1980, ch. 7; B. F. G. Johnson, *Adv. Dynamic Stereochem.*, 1988, **2**, 207; L. J. Farrugia, in *Comprehensive Organometallic Chemistry II*, eds. G. Wilkinson, F. G. A. Stone and E. W. Abel, Pergamon, Oxford, 1995, vol. 10, p. 187.

22 J. B. Keister, M. W. Payne and M. Muscatella, *Organometallics*, 1983, **2**, 219.

23 R. A. Brice, S. C. Pearse, I. D. Salter and K. Henrick, *J. Chem. Soc.*, *Dalton Trans.*, 1986, 2181.

24 A. J. Amoroso, A. J. Edwards, B. F. G. Johnson, J. Lewis, M. R. Al-Mandhary, P. R. Raithby, V. P. Saharan and W. Tak Wong, *J. Organomet. Chem.*, 1993, **443**, C11.

25 T. Adatia, G. Conole, S. R. Drake, B. F. G. Johnson, M. Kessler, J. Lewis and M. McPartlin, *J. Chem. Soc.*, *Dalton Trans.*, 1997, 669.

26 J. T. Mague and C. L. Lloyd, *Organometallics*, 1992, **11**, 26.

27 E. W. Abel, S. K. Bhargava and K. G. Orrell, *Prog. Inorg. Chem.*, 1984, **32**, 1.

28 B. E. Mann, in *Comprehensive Organometallic Chemistry*, eds. G. Wilkinson, F. G. A. Stone and E. W. Abel, Pergamon, Oxford, 1982, ch. 20.

29 D. F. Shriver, *The Manipulation of Air-Sensitive Compounds*, McGraw-Hill, New York, 1969.

30 R. Uson and A. Laguna, *Organomet. Synth.*, 1986, **3**, 315.

31 G. E. Coates and C. Parkin, *J. Chem. Soc.*, 1962, 3220.

32 V. Šik, Ph.D. Thesis, University of Exeter, 1979.

33 D. A. Kleier and G. Binsch, *J. Magn. Reson.*, 1970, **3**, 146; DNMR 3, Program 165, Quantum Chemistry Exchange, Indiana University, 1970.

34 SHELXTL PC, version 5.03, Siemens Analytical X-Ray Instruments, Madison, WI, 1994.

35 A. G. Orpen, *J. Chem. Soc.*, *Dalton Trans.*, 1980, 2509.

36 G. M. Sheldrick, SHELX 76, Program for Crystal Structure Determination, University of Cambridge, 1976.

37 N. Walker and D. Stuart, *Acta Crystallogr.*, *Sect. A*, 1983, **39**, 158.

Received 21*st October* 1997; *Paper* 7/07585E